ELSEVIER

International Journal of Mass Spectrometry 202 (2000) 81–89

International Journal of Mass Spectrometry

Peak shape for a quadrupole mass spectrometer: comparison of computer simulation and experiment

K. Blaum[a,*], Ch. Geppert[a], P. Müller[a], W. Nörtershäuser[b], K. Wendt[a], B.A. Bushaw[b]

[a]*Institut für Physik, Johannes Gutenberg-Universität Mainz, D-55099 Mainz, Germany*
[b]*Pacific Northwest National Laboratory, Richland, WA 99352, USA*

Received 24 January 2000; accepted 28 February 2000

Abstract

Computer simulations of ion trajectories have been used to evaluate the performance of a quadrupole mass spectrometer. Consideration has been given to realistic fields modeled on a commercial system as well as experimental distributions with respect to ion entry position, axial and radial velocity and relative phase of the quadrupole field. Determination of the mass filter acceptance-area as a function of the mass setting yields mass peak shapes with a dynamic range of more than seven orders of magnitude and thus provides estimates for abundance sensitivity. Results from these simulations are found to give excellent agreement with experimental measurements for different elements in a wide mass range of $6 \leq A \leq 160$. Further, conventional Monte Carlo simulations give insight into subtle effects resulting in a substructure on the top of the mass peak and allows the determination of the energy spread of the initial ion ensemble. (Int J Mass Spectrom 202 (2000) 81–89) © 2000 Elsevier Science B.V.

Keywords: Quadrupole mass filter; Ion energy distribution; Ion trajectory calculations; Isotopic abundance sensitivity; Peak shape

1. Introduction

Since the development of the radio frequency (rf) quadrupole mass filter (QMF) by Paul and co-workers in the 1950s [1–3], quadrupole mass spectrometers (QMSs) have become increasingly popular in a wide range of scientific fields. Because of this popularity, and the desire to gain a better understanding of the performance attainable under a wide variety of conditions, there have been many experimental and theoretical investigations. Most of the earlier theoretical work with analytical expressions required the assumption of idealized spatial and/or temporal fields as well as ion distributions (for an overview see [4] and references therein). The development of powerful computers now permits more advanced simulation studies that use realistic models for the description of the QMF field [5–11]. Thus, the influences of spatial and temporal field imperfections [12–15] on the performance can be studied in detail.

In a prior publication, we have analyzed the potential distributions of different real QMS geometries and compared their performance to an ideal instrument [11] using the program SIMION 3D version 6.0 [16]. Ion trajectory simulations were used to calculate spatial and angular acceptance of ions en-

* Corresponding author. E-mail: K.Blaum@Larissa.physik.uni-mainz.de

1387-3806/00/$20.00 © 2000 Elsevier Science B.V. All rights reserved
PII S1387-3806(00)00237-2

tering the QMF. Evaluation of the changes in acceptance as a function of the QMF operating parameters at discrete neighboring mass* values yielded predictions of isotopic abundance sensitivity, which were confirmed by comparison with experiment. However, a detailed understanding of the mass peak structure is necessary for precise isotope ratio measurements. Thus in this work, we have extended the acceptance-area method to obtain a comprehensive description of the mass peak shape. Additionally, a more conventional Monte Carlo approach has been used to investigate substructures that are observed over the peak tops. We compare the results of the simulations with high-dynamic-range measurements ($>10^7$) of peak shapes, carried out for different elements covering the mass range of $6 < A < 160$. For these studies, a commercial QMS system has been used under a variety of experimental working conditions including electron impact (EI) and laser ionization. For all conditions, the experimentally observed mass peak shapes show excellent agreement with the simulations over many orders of magnitude. Furthermore, the disappearance of the substructure at low ion energies could be used to determine the energy spread of the ion ensemble.

2. Theory

To develop an understanding of the shape of peaks transmitted through a linear QMF, we must begin with a short review of the standard design and theory of these devices. More detailed descriptions can be found in numerous papers and textbooks (see e.g. [1,3,4,17]). The ideal QMF would be a structure of four infinitely long parallel electrodes of hyperbolic cross section to which a sinusoidal potential is applied. This potential is composed of a dc component (amplitude U) and a rf component (amplitude V, angular frequency ω), which results in the quadrupolar electric field distribution

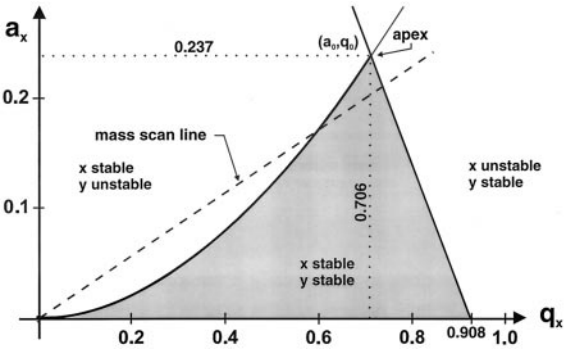

Fig. 1. The region of simultaneous x and y stability in the (a_x, q_x) plane, as used for quadrupole mass filter operation showing a typical mass scan line.

$$\Phi(x, y, t) = (U - V \cos \omega t) \frac{x^2 - y^2}{r_0^2} \tag{1}$$

where r_0, known as the free-field radius, is the distance from the symmetry axis to the electrode surfaces. For this idealized potential, the equations of motion for an ion with mass-to-charge ratio m/Ze injected along the z axis are described in the x and y coordinates by the generalized Mathieu equation [18]

$$\frac{d^2u}{d\xi^2} + [a_u - 2q_u \cos(2\xi)]u = 0 \tag{2}$$

where u represents either x or y and $\xi = \omega t/2$ and $d^2z/d\xi^2 = 0$. The trajectories of the ions and the operating parameters are expressed as functions of the dimensionless variables a_u and q_u, which are related to the potentials U and V according to

$$a_u = a_x = -a_y = \frac{8ZeU}{mr_0^2\omega^2} \tag{3}$$

$$q_u = q_x = -q_y = \frac{4ZeV}{mr_0^2\omega^2}$$

The ion trajectories are stable, i.e. of bounded amplitude in the x and y dimensions, only for limited values of a_u and q_u as shown in the stability diagram in Fig. 1. Note that ions of lower mass are unstable only in the x direction and ions of higher mass are unstable only in the y direction.

The dependence of a_u and q_u on m/Z in the

* Since we deal only with singly charged ions, we use the mass number A to refer implicitly to the ratio of mass to charge numbers. Where actual masses and charges are required, m and Ze are used.

relations (3) is the basis for the operation of the QMF as a band-pass mass filter, which commonly uses the region in the vicinity of the apex in the stability diagram. Simultaneously scanning the amplitudes of U and V along a "mass scan line" of fixed ratio $U/V \equiv a_u/2q_u$ through the stability region, as indicated in Fig. 1, produces a mass spectrum with constant resolution $\Re = m/\Delta m$. By increasing the U/V ratio, the transmitted mass range Δm is narrowed, and hence $\Re$ is increased. In this constant resolution mode, the width of the peaks obviously changes with mass. Often this is not desirable and one would like to have constant Δm over a given mass range. To do this precisely over large mass ranges requires a parametric adjustment of the U/V ratio, however, over limited mass ranges, a constant Δm mode can be approximated by adding a constant offset to U [4]. We use this constant Δm mode of operation for our QMS and the U offset value is specifically considered in the simulations.

The real QMF will have a number of imperfections that will cause deviations from the ideal behavior. These include finite dimensions, the substitution of circular cross-section electrodes for the ideal hyperbolic form, and various misalignments. These imperfections have been discussed in detail in [11] while this paper addresses the affect on the overall shape of a mass peak, as is outlined in Fig. 2. The transmitted range Δq_u of the mass scan line is given in Fig. 2(A) and the ideal QMF, as discussed above, should yield a rectangular shaped mass peak, as shown in Fig. 2(B). It is possible for ions with nominally stable trajectories to undergo oscillations that would become larger than the finite free-field radius; the ion then impacts an electrode and is not transmitted. This becomes more pronounced for ions entering further away from the z axis, as well as for (a_u, q_u) values near the boundaries of the stability region. Due to the different class of oscillations experienced in x and y coordinates, this effect is more pronounced on the higher mass side. Thus the flat-top peak becomes asymmetrically rounded with the peak maximum shifted slightly to the lower mass side, as shown in Fig. 2(C). With the finite length of a real QMF, an ion with nominally unstable trajectory, but starting within

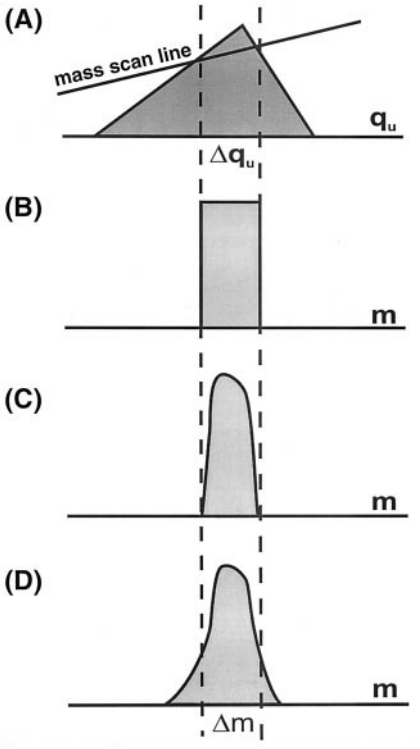

Fig. 2. Evolution of real mass peak shapes. Shown are the apex of the first stability region (A) and expected peak shapes for ideal infinite field (B), only transverse-limited field (C), and finite field limited in transverse and longitudinal dimensions (D).

a small but finite area close to the symmetry axis, will experience defocusing forces that are too small to cause rejection during the transit time. This results in tails on the mass peaks, which are more pronounced on the low mass side (again because of the different oscillation classes), as is shown in Fig. 2(D). The peak shape can be further distorted by fringing fields at the entrance and exit of the device [6,7,12,14] as well as by other field imperfections, such as those arising from using circular electrodes [4,11]. The latter lead to nonlinear resonances, which may be observed as additional narrow structures on the mass peak. The exact location where individual nonlinear resonances appear can be evaluated using a multipole expansion of the QMF field distribution [13,19]. It is important to emphasize that our approach does not solve the Mathieu equations, in either the simple first-order form or considering the higher-order multipole expan-

sions. Rather, field modeling based on actual geometries is used to calculate electrostatic forces for subsequent ion trajectory simulations, as described in Sec. 3.

3. Simulations

The ion trajectory simulation program SIMION 3D [16] is a PC based package for designing and analyzing ion optics with three-dimensional (3D) electrostatic potential and/or magnetic field arrays. The field-induced forces are then used for ion trajectory calculations. User programming permits modeling dynamic devices like the QMF or an ion trap. We have written subroutines that control variation of all parameters of the device and the starting ion conditions. These include dc and ac voltage, the radio frequency and its phase, ion mass, and the initial position in phase space of each individual ion in an ensemble.

The QMS system is divided into three major component regions: the ion source and ion optics at the entrance, the mass filter section (QMF), and the detector region with the post acceleration field. These have been described in detail in [11]. Consideration of the complete system allows proper treatment of fringing fields at the QMF entrance and exit apertures, which are known to influence transmission characteristics strongly [6,7,12,14,20]. All simulations were carried out in full 3D representation with a resolution of 50 μm. This is sufficient resolution to reproduce minor field imperfections, caused by circular electrodes, that induce nonlinear resonances in the ion oscillations. For all simulations, a beam divergence of 6° and a beam radius of 0.6 mm at the entrance to the QMF have been used. These parameters result from modeling of the ion source and extraction optics under realistic operating conditions [11]. The simulation results have been used in two distinctly different approaches for characterizing QMF performance. The first determines transmission of ions through the QMF and uses conventional Monte Carlo methods to evaluate fine details of the peak structure, however the number of calculated ion trajectories obviously limits the dynamic range that can be achieved. The second performs a series of simulations to determine the boundaries of the ion acceptance area and can provide results over a high dynamic range.

A detailed description of the acceptance-area method for calculating the transmission of the QMF at a single point in the (a_u, q_u)-parameter space has been given in [11]. When set for a given mass number A, trajectory simulations can be used to determine an area in the x–y plane at the entrance of the QMF for which ions of a given mass number A' are transmitted. At the desired mass ($A' = A$) we denote this acceptance area M_{stable}. Due to the finite length of the QMF, unstable ions of a different mass will still have a small but finite acceptance area M_{unstable} located close to the QMF axis, where defocusing forces of the field are too small to cause rejection. The ratio $M_{\text{stable}}/M_{\text{unstable}}$ then gives an estimate of the selectivity of the system. In [11], we examined the transmission of an ion of mass number A at discrete points along the mass scan line corresponding to A and $A \pm \frac{1}{2}$. In this work, the procedure has been automated to calculate the transmission over a continuous mass range, at a user-defined resolution, resulting in a prediction of the complete mass spectrum. Additionally, the earlier calculations only considered monoenergetic ions with distribution of entry position in the x–y plane and randomized rf phases; this work includes additional distributions in the entrance angle (beam divergence) and a distribution of ion energies.

4. Experimental

The experimental apparatus used in these studies has been discussed in [11] and only a brief description is given here. The QMS is a commercial system (ABB Extrel, Pittsburgh, USA) with 9.39 mm radius rods of 21 cm length and a free-field radius of $r_0 = 8.33$ mm. The system can be driven by different power supplies at frequencies of either 2.9 MHz ($A \leq 64$) or 1.2 MHz ($A \leq 500$). Ions transmitted through the QMF are detected by an off-axis continuous dynode secondary electron multiplier. For the measurements reported here, metallic lithium, calcium or gadolinium

were loaded into an electrothermally heated graphite crucible of 2.5 cm length and 2.6 mm inner diameter. At temperatures of 500–700 °C (Li and Ca) or 1200–1400 °C (Gd) these metals are evaporated at a suitable rate. We use a standard EXTREL crossed-beam EI ion source with the atomic beam directed along the quadrupole axis. When EI ionization is used, the electron energy is kept at 8–10 eV to avoid most molecular interferences. Because of their lower ionization potentials, the metals studied are still efficiently ionized at these EI energies. For calcium, some additional measurements were carried out using resonant laser ionization within the same interaction volume.

5. Results and discussion

In this section two different types of simulations are compared with experimental measurements. First we examine the detailed structure over the peak top using Monte Carlo methods. Then, the overall shape is evaluated at high dynamic range using acceptance-area simulations.

Fig. 3 shows detailed measurements of the ^{40}Ca mass peak with resolution $\Re \sim 100$ obtained with (A) laser and (B) EI ionization, plotted on a normalized logarithmic scale. Laser ionization was carried out with single-mode cw-laser excitation on the 422.7 nm resonance line of Ca I with subsequent nonresonant ionization at 363.8 nm [21]. The points connected by dotted lines are the experimental data while the solid lines are the results of simulations. These simulations computed 1000 ion trajectories for each point, at a resolution of 0.01 mass units. The mean ion energy, both experimental and in simulations, was ~9 eV. Although the width and tail structure for both experimental mass peaks are quite similar, the structure on the top has apparent differences. The observed structure in (A) is attributed to having the QMS exit aperture radius slightly smaller than r_0 (which is the case for almost all commercially available instruments). If the initial ion energy distribution is narrow, the ion motion will have a nearly stationary wave shape. This is illustrated with simulated trajectories

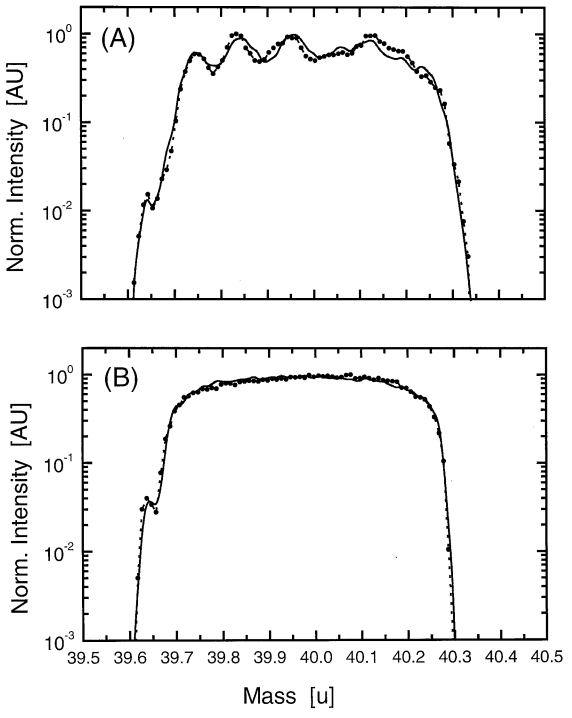

Fig. 3. Transmission peak shapes obtained by laser ionization (A) and EI ionization (B) of ^{40}Ca. Experimental results are shown as points connected by dotted lines and peak shapes calculated with Monte Carlo simulations as solid lines. Input parameters and energy uncertainties are discussed in the text.

for monoenergetic ions shown in Fig. 4(A). The exact location of the motion amplitude extrema are only weakly dependent on the initial rf phase (which has been varied for the different traces in Fig. 4). Also, the entry radial displacement and velocity only affect the amplitude of the ion motion, but not the extrema positions. However, the period, and hence the coincidence of the extrema with the exit aperture, depends on the exact working (a_u, q_u) parameters and axial velocity of the ion. The effect of slightly reducing the q_u parameter is illustrated in Fig. 4(B). Thus, during a mass scan, which corresponds to changing q_u, the motion amplitude maxima and minima will be scanned across the exit aperture and impose variations on the observed transmission. Note that the pattern will be complicated by the fact that the frequency of the macrocycles is different in the *x* and *y* dimensions. A distribution of axial velocities corresponds to a

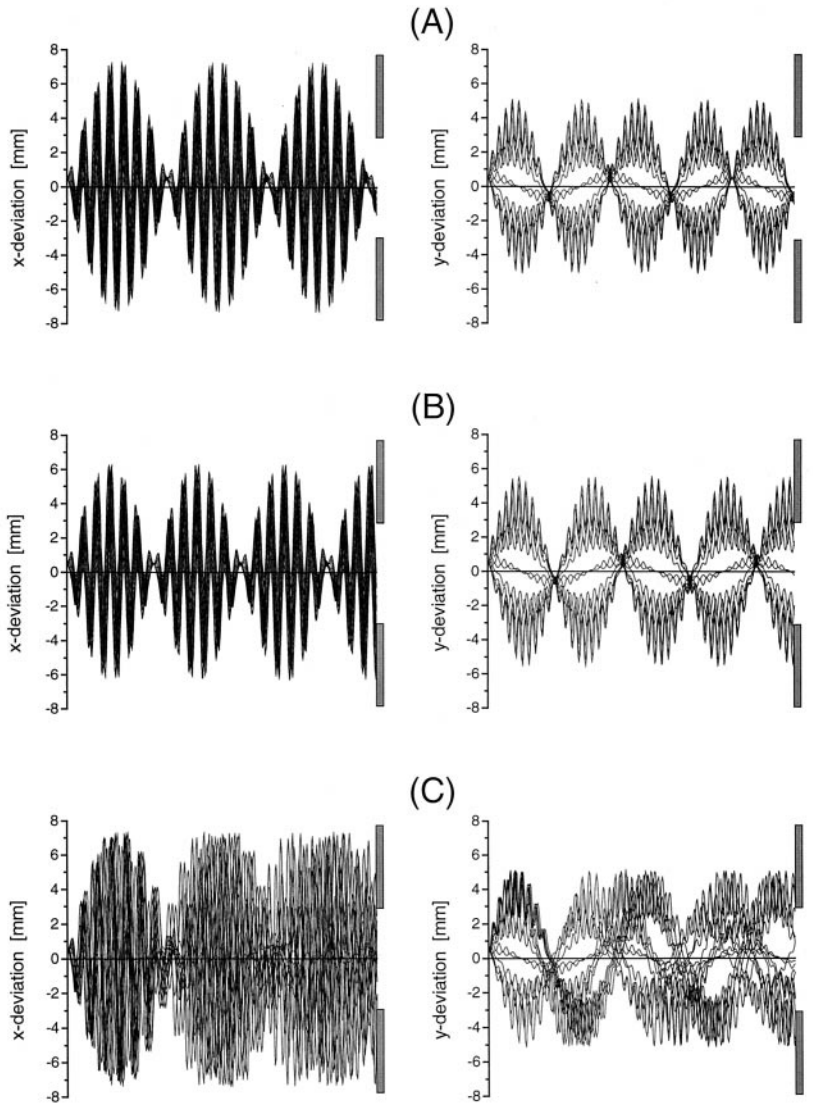

Fig. 4. Projections of thirteen ion trajectories onto the x–z (left column) and the y–z plane (right column) with different initial phases of the rf field, equally spaced between 0 and 2π. (A) and (B) show results for monoenergetic ions, while in (C) the effect of an energy spread of 1.3 eV is illustrated. The operating points (a_x, q_x) are (0.23, 0.7085) in (A) and (C) and (0.23, 0.706) in (B). In each case ion mass is 40 u, mean ion energy is 9 eV, and ion entry is parallel 0.5 mm from the symmetry axis in both dimensions.

distribution of ion energies. This leads to a smearing out of the stationary wave pattern, as shown in Fig. 4(C) where conditions are the same as in Fig. 4(A) except that an energy uncertainty of 1.3 eV has been used. For a given mean energy, a certain energy spread will have the lowest and highest energy ions shifted by one-half period of the macrocycle motion at the exit aperture. Above this point, the structure over the top of the mass peak is largely expected to disappear. A series of simulations were performed as a function of mean energy to determine the energy width required for removal of the structure, with results listed in Table 1. As might be expected from energy–velocity relations, the required energy width

Table 1
Energy shift ΔE, necessary to produce a shift of one-half period in the macromotion for different mean ion energies E; uncertainty values arise from considering a distribution of starting conditions

Mean ion energy E (eV)	Energy spread ΔE (eV)
15	2.4 ± 0.2
12	1.4 ± 0.1
11	1.2 ± 0.1
10	1.0 ± 0.1
9	0.8 ± 0.1
8	0.75 ± 0.1
7	0.7 ± 0.1
6	0.6 ± 0.1
5	0.45 ± 0.05

increases approximately quadratically with the mean ion energy. Thus, if spectra are recorded at increasing ion energies, the point at which the structure disappears can be used to estimate the energy spread of the source.

In Fig. 3(A), which is obtained by laser ionization (LI) a strong structure on the peak top is observed, with transmission fluctuation of up to 30%. The observed structure could be well reproduced in simulation simply by adjusting the width of the ion energy distribution to $\Delta E_{\mathrm{LI}} = 0.4$ eV. The peak width and the precise positioning of the substructure are very sensitive to the values of U and V. Thus, these were checked and adjusted against the experimentally observed peak width and centroid. The resulting values were then used for all further calculations of detailed peak structure. Fig. 3(B) shows the peak shape obtained with EI ionization and the same mean ion energy as the laser ionization in Fig. 3(A) and the observed peak shape is quite smooth without structure over the top. Using Table 1 and additional measurements at other ion energies, the energy spread was estimated to be $\Delta E_{\mathrm{EI}} = 1.3$ eV. This value was used for the simulated curve shown in Fig. 3(B) and gives excellent agreement with the experimental peak shape. The energy width is much larger than that found for laser ionization and is attributed to space charge from the electron beam in the ionization volume. The only significant structure remaining in the EI spectrum is a weak dip in the rising edge. This dip is also present in the laser ionization spectrum and is ascribed to a coincidence of non-linear resonances arising from a combination of sixth- and tenth-order components of the multipole expansion of the field. These coupled nonlinear resonances make the ion trajectory unstable and thus result in strongly reduced transmission.

For comparison between the acceptance-area simulations and experiments, high dynamic-range mass spectra were recorded under optimized working conditions. The resulting spectra for masses in the range of lithium (A), calcium (B), and gadolinium (C) are shown on a normalized logarithmic scale in Fig. 5. The experimental points were obtained with conventional EI ionization. During each scan the QMF was operated in constant Δm mode, where Δm is defined as the peak width at 10% height. For Li and Gd $\Delta m \sim 0.65$ while for Ca $\Delta m \sim 0.4$, which, in each case, provides a practical compromise between transmission and abundance sensitivity. Thus the resolution values are approximately 11, 100, and 250 at $A = 7$, 40, and 158, respectively. The background peaks observed at mass numbers 39 and 41 are attributed to potassium, which has an ionization potential lower than that of calcium and thus cannot be suppressed by the low EI energy. The Gd spectrum was recorded using a rf frequency of 1.2 MHz, which was necessary to reach the higher masses involved. Due to the refractory nature of Gd, only moderate evaporation rates could be achieved and thus the dynamic range is several orders of magnitude lower than with Li or Ca. Further, with the 1.2 MHz operation the tails of the Gd mass peaks do not fall off as quickly.

For acceptance-area simulations corresponding to these experimental measurements, fixed input parameters were ion energy of 9 eV with $\Delta E_{\mathrm{EI}} = 1.3$ eV, while the U/V ratio was adjusted to give a best fit to the experimentally observed Δm. Under these conditions, no substructure is observed over the peak tops, as has been discussed above. The resulting transmission functions for $A = 7$, 40, and 158, are shown as solid lines in Fig. 5 and the agreement with the observed experimental peaks is very good over eight orders of magnitude. The agreement for the peak

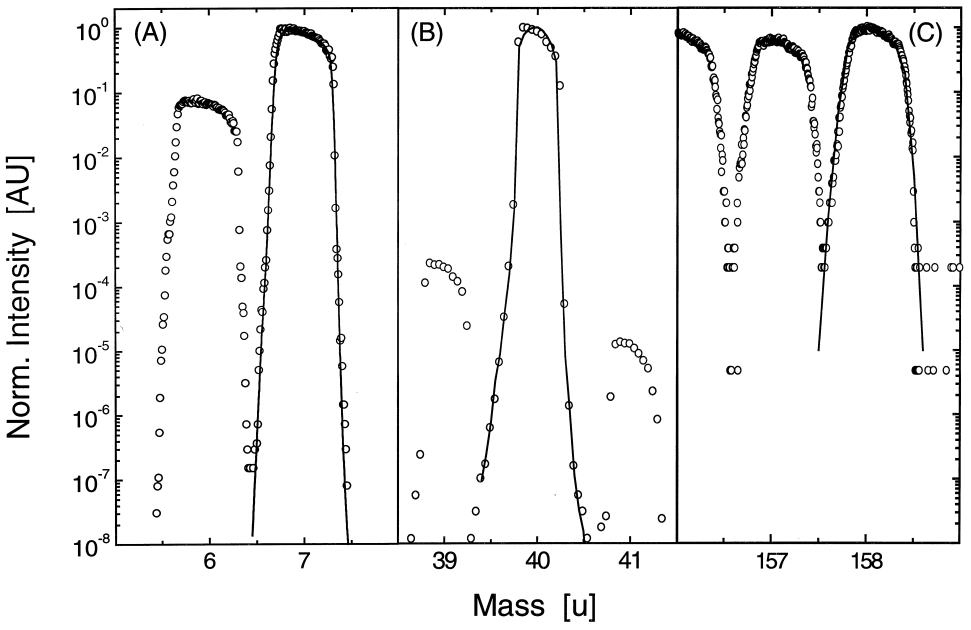

Fig. 5. High-dynamic-range mass spectrum in the range of lithium (A), calcium (B) and gadolinium (C). Experimental results (points), obtained using selective EI ionization, are compared to peak shapes simulated with the acceptance-area method (solid lines). All parameters are discussed in the text.

wings is particularly important, indicating that the simulations can give reliable a priori estimates of abundance sensitivity. As explained in Fig. 2, the peak shape in both experiment and theory is somewhat asymmetric with the maximum shifted slightly to lower mass. At smaller Δm, as is the case for $A = 40$, there is less of the nearly flat region on the top of the peak.

6. Conclusion

Ion trajectory simulations have been performed to model mass peaks of a commercial QMS system. A comprehensive description of the peak shape was obtained by evaluating the acceptance-area of the QMF as a function of the mass setting. This approach accurately reproduced experimentally observed peak shapes over a dynamic range of up to eight orders of magnitude and the mass range of $6 \leq A \leq 160$. Substructures on the mass peak top are understood as arising from the ion macromotion in the QMF, whose pattern becomes nearly stationary for an ensemble with a narrow energy distribution. Location and size of the induced transmission extrema were calculated for different ion sources using a Monte Carlo approach and agreed very well with experimental results. Furthermore, the energy dependence of this structure has been used to determine the energy width of ion ensembles created by EI and laser ionization. Consideration of these effects is particularly important for isotope ratio measurements using laser ionization, where an ion ensemble with a small energy spread is created.

Acknowledgements

The authors would like to thank Dr. R. E. Pedder and G. York of ABB Extrel for their outstanding support and many stimulating discussions. Funding from the Deutsche Forschungsgemeinschaft and the “Zentrum für Umweltforschung der Johannes Gutenberg-Universität Mainz” is gratefully acknowledged.

Support for one of the authors (B.A.B.) was provided by the U.S. Department of Energy, Office of Science.

References

[1] W. Paul, H. Steinwedel, Z. Naturforsch. A8 (1953) 448.
[2] W. Paul, M. Raether, Z. Phys. 140 (1955) 162.
[3] W. Paul, H.P. Reinhard, U. von Zahn, Z. Phys. 152 (1958) 143.
[4] P.H. Dawson (Ed.), Quadrupole Mass Spectrometry and its Applications, American Institute of Physics, New York, 1995; originally published by Elsevier, Amsterdam, 1976.
[5] C. Hägg, I. Szabo, Int. J. Mass Spectrom. Ion Processes 73 (1986) 295.
[6] K.L. Hunter, B.J. McIntosh, Int. J. Mass Spectrom. Ion Processes 87 (1989) 157.
[7] B.J. McIntosh, K.L. Hunter, Int. J. Mass Spectrom. Ion Processes 87 (1989) 165.
[8] F. Muntean, Int. J. Mass Spectrom. Ion Processes 151 (1995) 197.
[9] F. Muntean, D. Ursu, N. Lupsa, Vacuum 46 (1995) 131.
[10] A.J. Reuben, G.B. Smith, P. Moses, A.V. Vagov, M.D. Woods, D.B. Gordon, R.W. Munn, Int. J. Mass Spectrom. Ion Processes 154 (1996) 43.
[11] K. Blaum, Ch. Geppert, P. Müller, W. Nörtershäuser, E.W. Otten, A. Schmitt, N. Trautmann, K. Wendt, B.A. Bushaw, Int. J. Mass Spectrom. Ion Processes 181 (1998) 67.
[12] W.M. Brubaker, Adv. Mass Spectrom. 4 (1968) 293.
[13] P.H. Dawson, N.R. Whetten, Int. J. Mass Spectrom. Ion Phys. 3 (1969) 1.
[14] P.H. Dawson, Int. J. Mass Spectrom. Ion Phys. 6 (1971) 33.
[15] P.H. Dawson, Int. J. Mass Spectrom. Ion Phys. 14 (1974) 317.
[16] D.A. Dahl, SIMION 3D 6.0, Ion Source Software, Idaho National Engineering Laboratory, 1995.
[17] G.E. Lee-Whiting, L. Yamazaki, Nucl. Instrum. Methods 94 (1971) 319.
[18] N.W. McLachlan, Theory and Application of Mathieu Functions, Clarendon, Oxford, 1947.
[19] F. von Busch, W. Paul, Z. Phys. 164 (1961) 588.
[20] P.H. Dawson, Int. J. Mass Spectrom. Ion Phys. 17 (1975) 423.
[21] W. Nörtershäuser, N. Trautmann, K. Wendt, B.A. Bushaw, Spectrochim. Acta B 53 (1998) 709.